Rotational and deperturbation analyses of the (0,0) and (1,0) vibrational bands of the [15.30]1 – $X\,^3\Sigma^-(0^+)$ transition of WS

Kristin N. Bales,[1] Jack C. Harms,[1] James J. O'Brien,[1] and Leah C. O'Brien[2,a]

AFFILLIATIONS

[1]*Department of Chemistry and Biochemistry, University of Missouri – St. Louis, Saint Louis, MO 63121, USA*

[2]*Department of Chemistry, Southern Illinois University Edwardsville, Edwardsville, IL 62026, USA*

[a]Author to whom correspondence should be addressed: lobrien@siue.edu

ABSTRACT

The (0,0) and (1,0) bands of the [15.30]1 – $X\,^3\Sigma^-(0^+)$ transition of tungsten sulfide (WS) were recorded at high resolution using intracavity laser spectroscopy integrated with a Fourier-transform spectrometer for detection (ILS-FTS). The target WS molecules were produced in the plasma discharge of a tungsten-lined copper hollow cathode, using a gas mixture of approximately 70% Ar and 30% H_2, with a trace amount of CS_2. The total pressure in the reaction chamber was about 1 torr. Evidence of heterogeneous mass- and J-dependent perturbations was observed in each spectrum for all four abundant isotopologues: $^{182}W^{32}S$, $^{183}W^{32}S$, $^{184}W^{32}S$, and $^{186}W^{32}S$. The perturbations were attributed to interactions with the v=2 and v=3 vibrational levels of the $[14.26]0^+$ state of WS. A rotational analysis with deperturbation analysis was performed using PGOPHER to determine parameters for both states. A Dunham-like model which constrains parameters to expected mass relationships was used to describe the perturbed states.

1. INTRODUCTION

The complex electronic structure of tungsten monosulfide, WS, has recently been a focus of attention for *ab initio* and spectroscopic studies.[1-8] Industrial interest in the W-S bond has arisen from the possibility of using the semiconducting material WS_2 in nanoelectronic devices and solar cells.[9,10] From an academic perspective, the large number of electrons and accessible valence orbitals give rise to a molecule that is very difficult to model computationally, with many electronic states and a high potential for interactions between states. Thorough spectroscopic analysis of the molecule experimentally can enable a deeper understanding of this complex electronic landscape. This understanding can inform future uses of materials like WS_2, as well as guide the development of more robust computational methods.

Early work with the WS molecule began with relatively low-level DFT calculation of electronic states, relative energies, and bond lengths by Liang and Andrews in 2002.[1] In 2017, Sevy, *et al.* provided more DFT calculations and measured the bond dissociation energy of WS using resonant two-photon ionization spectroscopy.[2] The most comprehensive work to date on the molecule came in 2019 when Tsang *et al.* provided a set of high level *ab initio* calculations alongside experimental observations collected using laser induced fluorescence (LIF) with rotational analyses of several electronic transitions.[3] Two additional works by Zhang, *et al.* followed soon after, investigating the spin-spin splitting of the $^3\Sigma^-(0^+)$ ground state,[4] the observation of additional low-lying states, and updated computational results.[5] Our group also has contributed significantly to the body of spectroscopic work, with papers reporting the analysis of additional electronic transitions observed using intracavity laser spectroscopy with Fourier-transform spectrometer detection (ILS-FTS).[6-8]

The $[15.30]1 - X\,^3\Sigma^-(0^+)$ transition was first observed[4] using LIF spectra collected from a molecular beam. The low temperature of that technique inherently limits observation of rotational structure to low-J transitions. This differs significantly from the spectra obtained using a hollow cathode discharge: in many cases, rotational branches extend to J>100 when observed in absorption using ILS. Additionally, that initial analysis only determined parameters for the most abundant isotopologue, $^{184}W^{32}S$, because the isotopologue structure could not be resolved for low-J lines in the (0,0) band. This structure is more apparent in the high J transitions observed at Doppler limited resolution using ILS-FTS: rotational structure for each abundant isotopologue of WS has been observed and identified in absorption using ILS-FTS.

In this work, the (0,0) and (1,0) bands of the $[15.30]1 - X(0^+)$ transition were recorded by ILS-FTS and rotationally analyzed using PGOPHER.[11] Rotational transitions were observed to very high J (J″>100) where isotopologue structure due to W could be clearly identified. A heterogenous perturbation[12] was observed in the P- and R-branches of each of these transitions, starting near J′=30. The strong Q-branch of each band was quite regular in appearance from low to high J. The observed perturbation is J-dependent: this dependence varies slightly for each isotopologue, perturbing the heaviest isotopologue ($^{186}W^{32}S$) at the lowest J-value. It is believed that the perturbing levels originate from excited vibrations of the $[14.26]0^+$ state, which was characterized by our group previously.[7] Newly measured lines for the (2,0) and (3,0) bands of the $[14.26]0^+ - X(0^+)$ transition were added to this fit and used to assist in a deperturbation

analysis of the [15.30]1 state. The $X(0^+)$, [15.30]1, and [14.26]0^+ states were fit to a mass-independent Dunham model[13] using a constrained variables approach.[14] The vibrational dependence of the $X(0^+)$ and [14.26]0^+ states was determined by including line positions of the (1,0), (0,1), and (1,2) bands of the [14.26]0^+ - $X(0^+)$ transition from our previous analysis.[7] The Dunham model required slight corrections to the vibrational term energies for each isotopologue. In general, these corrections are quite small (0.05-1.5 cm^{-1}), especially if one considers that the Dunham model is only appropriate for a "smooth" potential, and that the [14.26]0^+ and [15.30]1 states are known to interact. The final fit included line positions from Harms *et al.*[6] and Tsang *et al.*[3] of transitions involving the $X(0^+)$ state to minimize correlation of parameters between all three states. Results of this deperturbation analysis, including the determined molecular constants for the three involved electronic states, are presented here.

2. EXPERIMENTAL METHODS

Experimental spectra were collected at the University of Missouri – St. Louis using the ILS-FTS dye laser system that has been previously described in detail.[6,15] Target molecules were produced in the plasma discharge created by applying an electrical current of 0.15 A to a 25 mm W-lined copper hollow cathode, in the presence of approximately 70% Ar, and 30% H_2, with a trace amount of CS_2. In this gas mixture, Ar is used as a sputter gas to vaporize W molecules from the surface of the cathode, and CS_2 provided sulfur for the reaction. The addition of H_2 has been found to increase the intensity of the transition, though the specific catalytic mechanism is unknown. The total pressure in the reaction chamber was about 1 torr.

In the ILS method, measurements are taken at a particular evolution time of the laser, called the generation time (t_g), which is controlled using an acousto-optic modulator (AOM). The AOM begins and ends the laser cycle via interruption of the CW Coherent Verdi V-10 pump laser. In these experiments, t_g values of 25 – 90 μsec were used, corresponding to effective pathlengths of 0.2 – 0.7 km. Operation of the ILS dye laser is synchronized to the data collection cycle of a Bruker IFS 125 M Fourier-transform spectrometer, which is used to record the ILS profile. For this analysis, a resolution of 0.01 cm^{-1} was used, corresponding to the calculated Doppler width of WS lines of 0.017 cm^{-1} (assuming a plasma temperature of approximately 500 K),[16] and each spectrum was composed of four coadded FTS scans. Spectra collected during operation of the plasma discharge were followed by collection of a background spectrum with no discharge present. Each experimental spectrum was divided by the corresponding background spectrum using Bruker's OPUS (v.8.5.29) software. For the weaker (1,0) band, a series of 20 partially overlapping experimental spectra were added together to increase the signal to noise ratio, then divided by the corresponding series of coadded background spectra, to give one continuous spectrum. All resultant experimental spectra were baseline corrected and calibrated as follows using the appropriate functions in PGOPHER.[11]

A beamsplitter allows dispersed ILS and ILS-FTS measurements to be recorded simultaneously. The line positions for the dispersed ILS measurements were verified to 0.005 cm^{-1} accuracy by collecting spectra from an extracavity I_2 cell at each monochromator location and calibrating those spectra using the data from Salami and Ross.[17,18] In the absence of suitable Ar I[19] or H_2O[20] lines typically used to calibrate ILS-FTS spectra, these ILS-FTS spectra were calibrated using unblended plasma lines identified in both the dispersed ILS and ILS-FTS

spectra. The internal precision of the ILS-FTS measurements is estimated to be near 0.001 cm^{-1}: as such, the wavenumber accuracy of the measurements is limited to the 0.005 cm^{-1} uncertainty of the reference I_2 data, but the fitting uncertainty is expected to be somewhat lower.

3. ANALYSIS AND RESULTS

Prominent red-degraded bandheads were observed at approximately 15,303 and 15,822 cm^{-1}. A much weaker bandhead was observed near 16,340 cm^{-1}. The band at 15,303 cm^{-1} was consistent with that observed previously by Zhang, *et al.*,[4] and the three bands were thus identified as the (0,0), (1,0), and (2,0) bands of the [15.30]1 – $X(0^+)$ transition. While the (0,0) and (1,0) bands were analyzed in this work, the (2,0) band was not strong enough to be included. Weaker bandheads within the (0,0) and (1,0) bands appeared at 15,265 and 15,784 cm^{-1} and were identified as belonging to the (1,1) and (2,1) bands, respectively. The prominent bands consisted of P-, Q-, and R-branches, consistent with a transition with $\Delta\Omega = \pm 1$ symmetry. Upon initial inspection, the (0,0) band showed a single, regular Q-branch and a single bandhead with no observable separation of abundant isotopologues, as expected. However, portions of the P- and R-branches were oddly irregular. Initial fitting of the Q-branch in PGOPHER[11] and comparison with simulations using previously determined parameters[7] suggested that higher J P- and R-lines were perturbed, resulting in an appreciable isotopologue shift that was fully resolved at Doppler limited resolution, as shown in Figure 1. Here, the Fortrat diagram of the PGOPHER[11] simulation indicates potential perturbations in the R-branch lines from roughly J=30 to J=60,

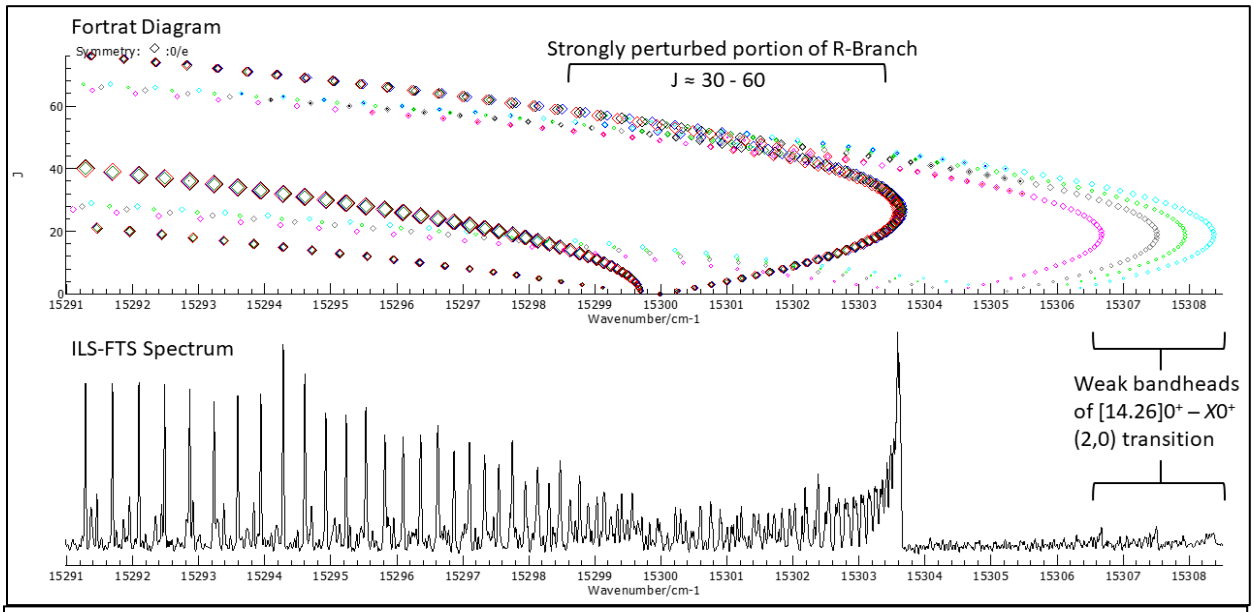

Figure 1. Fortrat diagram (upper panel) corresponding to the origin and bandhead regions of the (0,0) band of the [15.30]1 - $X\,^3\Sigma^-(0^+)$ transition with energy levels for v=2 of the [14.26]0^+ state included to illustrate the isotopologue-dependent perturbation observed in the R-branch of the experimental spectrum (lower panel). In contrast to this highly irregular portion, the left side of the figure shows the very regular and unperturbed portion of the P branch below J = 20, and the Q branch below J = 40, with lines for each isotopologue stacked together in this region. A temperature of 600 K was used for the PGOPHER simulation.

with isotopologues widely separated in this region. At higher and lower values of J, the P- and R-branch lines for each isotopologue are of nearly identical transition energy.

The perturbation in the rotational structure can be quite informative. Only P- and R-branches are affected in the [15.30]1 excited state and the ground state is 0^+; thus, the *e*-levels of the [15.30]1 state are being perturbed. This indicates that the perturbing state has symmetry $\Omega=0^+$. As found in the spectrum, the perturbation initially lowers the energy of the rotational levels as J increases, then suddenly raises the energy of rotational levels of the [15.30]1 state. This indicates that the perturbing state must be higher in energy and have a smaller rotational constant, B, to produce rotational energy levels that are initially higher than those of the [15.30]1 state then become lower in energy as J increases. The crossover point in the perturbed branches occurs between J'=35-50, with the exact J-value of the crossing dependent upon the isotopologue, as can be seen in Figure 2. The reduced energy level diagrams illustrate how the levels cross, including the specific J-value for the crossing point of each isotopologue. The perturbation interaction is strongest at these crossing points, producing large deviations from "regular" rotational structure. The vibrational constants are mass dependent, with the ^{186}WS isotopologue of lowest energy, and the ^{182}WS isotopologue of highest energy. The separation of these isotopologues will depend on Δv for a given transition. Generally, as Δv increases, the magnitude of the observed isotopologue shift will increase, with ^{186}WS moving lower and lower in energy compared to ^{182}WS. If Δv is negative, ^{182}WS will be lowest in energy and the magnitude of the shift is proportional to the magnitude of Δv. The magnitude of shift in J between isotopologues indicates that there must be a change in vibrational levels between the two interacting states. Consequently, the state(s) perturbing the [15.30]1 state must have v > 0.

In previous work with the WS molecule,[7] a Dunham-like model was used to describe the (1,0), (0,1), and (1,2) bands of the $[14.26]0^+ - X(0^+)$ transition. The (2,1) band of that transition was very strong, but a rotational assignment could not be secured due to overlap with the (1,0) band and some irregularity in branch structure. The clear irregularity in rotational structure seen in Figure 1 prompted the question: are these two excited states, v=2 of $[14.26]0^+$ and v=0 of [15.30]1, interacting with each other, complicating observed rotational structure and making branches difficult to track? The weak bandheads observed on the right side of Figure 1 are consistent in energy with the (2,0) band of the $[14.26]0^+ - X(0^+)$ transition predicted by the Dunham-like model. The simulated branch structure in the Fortrat diagram clearly illustrates a crossing of these two states between J=30-60. The perturbations in the (0,0) and (1,0) bands of the [15.30]1 transition were subsequently treated as interactions with the nearby v=2 and v=3 (respectively) levels of the $[14.26]0^+$ state of WS.

The L-uncouple operator was used to model the perturbation interaction in PGOPHER.[11] As described by Lefebvre-Brion and Field,[12] the L-uncouple operator is relevant in cases where there is a heterogeneous electronic-rotational perturbation between two states with ΔS=0, $\Delta\Omega=\pm1$ and $\Delta\Lambda=\pm1$. A heterogeneous interaction produces the previously described effects to the energy levels of the interacting states, which are also illustrated in panel B of Figure 2.

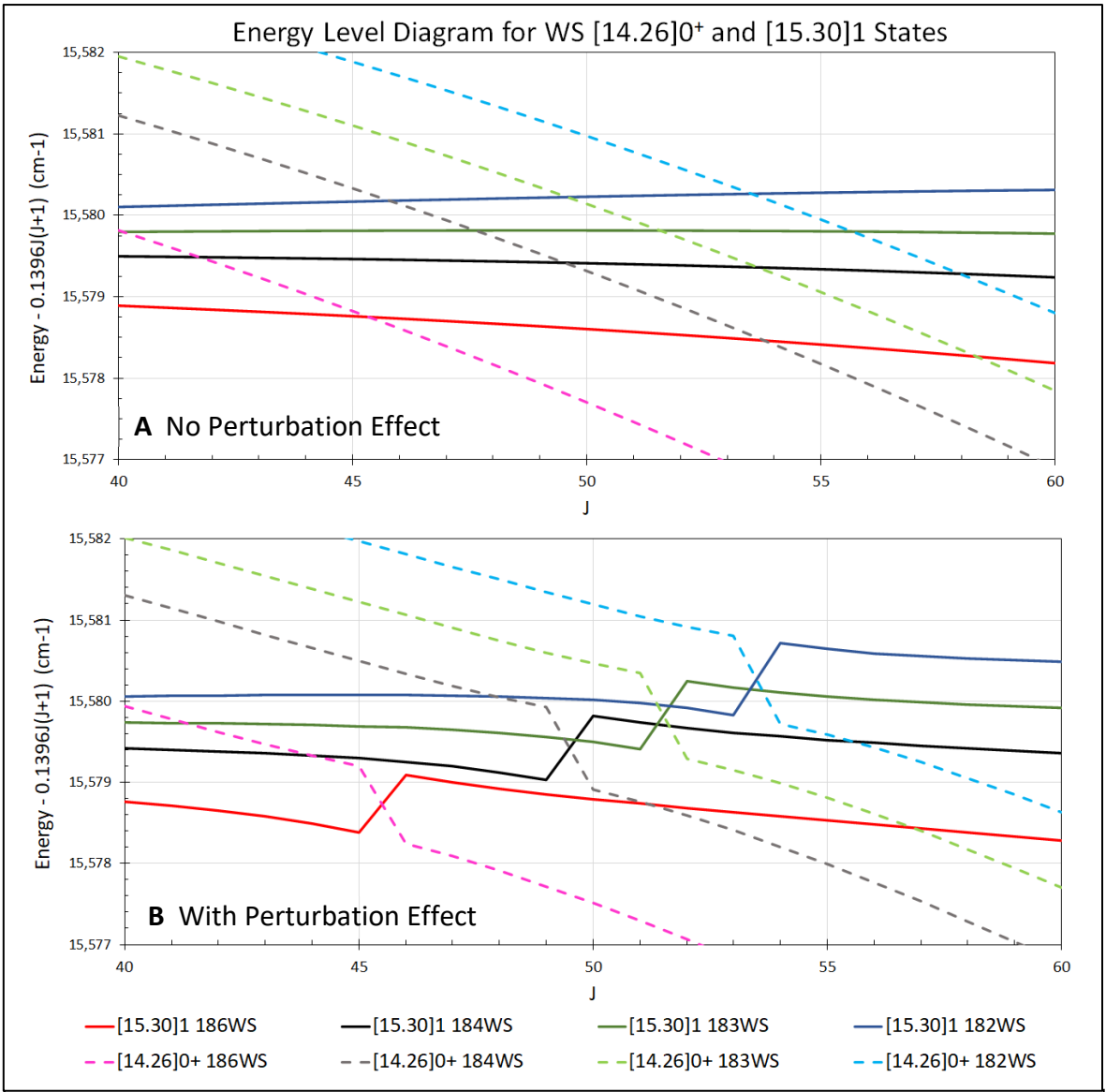

Figure 2. Reduced energy level diagram showing the energy level crossing region of v=2 of [14.26]0⁺ and v=0 of [15.30]1 states of WS. The ^{186}WS isotopologue energy levels cross at J" = 45, whereas the ^{182}WS isotopologue levels cross at J"=53. The top panel (A) shows the level crossing with no perturbation effect simulated, while the bottom panel (B) illustrates the effect of the perturbation on the energy levels of each state. The approximate B value of the v=0 of [15.30]1 state, 0.1396 cm^{-1}, multiplied by J(J+1) is subtracted from the overall energy of each state to allow easier visualization of the interactions.

Initial fitting of the perturbation was done on a band-by-band basis, with each isotopologue fit independently to its own set of parameters for each of the two electronic states. Included in the fit are lines from the (0,0), (1,0) and (1,1) bands of the [15.30]1 – $X(0^+)$ transition, as well as lines from the (1,0), (0,1), (1,2), (2,0), (2,1), and (3,0) bands of the [14.26]0^+ – $X(0^+)$ transition. The (1,0), (0,1), (1,2) band lines from the [14.26]0^+ transition were taken from the previous

analysis.[7] Line positions from our analysis of the (1,0) band of the [13.10]1 – $X(0^+)$ transition[6] as well as LIF line positions for the [12.37]1 – $X(0^+)$ and [13.10]1 – $X(0^+)$ transitions provided by Tsang *et al.*[3] were included to aid fitting accuracy of the ground state. Line assignments in the heavily perturbed portions of the spectrum were made with the aid of PGOPHER[11] models, and assignments were verified using Δ_2F values.[16] Because the upper state J' of any line R(J") is the same as that of P(J"+2), an R-branch line will be perturbed in the same direction and with the same magnitude as its corresponding P-branch line at J"+2. Using this concept, all assignments for perturbed lines were made in pairs, with corresponding lines compared to the expected unperturbed location from the initial PGOPHER simulation. This was particularly important in the heavily congested R-branch portion of the spectrum, where a corresponding P line (which was in a much less congested area of the spectrum) was required to verify line assignments. Also identified were 428 line positions from the perturbing [14.26]0^+ state, further supporting the assignments.

Following successful band-by-band fitting of the experimental data, a fully mass-independent Dunham fit was attempted. The constrained variables approach introduced by Breier and coworkers[14] and used by our group to model the $X(0^+)$ ground state of WS,[7] was used here for the ground state as well as the [14.26]0^+ and [15.30]1 states. Briefly, with this method, the Dunham parameters (Y_{00}, Y_{10}, Y_{01}, etc.) are added to PGOPHER[11] as variables which are used to define the PGOPHER[11] fitting parameters such as the Origin, B, and D values. Constraints are programmed into the PGOPHER[11] input file to relate the fitting parameters to Dunham relationships. The reference isotopologue in this analysis was the central $^{184}W^{32}S$, with the $Y_{l,m}$ Dunham parameters for the other three abundant species calculated from the central isotopologue using the relevant mass scaling.[7,14,21] While the rotational fine structure was modeled well by the expected mass relationships, there were small but significant deviations in the expected vibrational term energies, T_v. Consequently, ΔT parameters were incorporated into the fitting model to decouple the isotopologue-dependent T_v values from the Dunham expansion. These take the form:

$$Origin_v = Y_{00} + Y_{10} + Y_{20} + ... + \Delta T_v \tag{1}$$

$$B_v = Y_{01} + Y_{11} + Y_{21} + ... \tag{2}$$

$$D_v = Y_{02} + Y_{12} + Y_{22} + ... \tag{3}$$

where the Y_{lm} are the traditional Dunham parameters that fit the form

$$Y_{lm}^i = Y_{lm}^p \left(\frac{\mu_p}{\mu_i} \right)^{\frac{l}{2}+m} \tag{4}$$

where i and p indicate the individual and primary isotopologues, and μ is the reduced mass for the indicated isotopologue. These parameters describe the rovibrational structure of an ideal potential energy curve according to

$$T_{vJ}^{i} = Y_{lm}^{i}(v+\frac{1}{2})^{2}[J(J+1)]^{m} \quad (5).$$

The ΔT_v parameter in equation 1 indicates the magnitude of the deviation from the expected mass scaling shown in equation 4. These ΔT parameters decouple the isotopologue specific T_v values from the mass-dependent scaling of the vibrational Y_{10}, Y_{20}, …parameters predicted by the Dunham model. Consequently, they can be used to evaluate how well the Dunham model describes the "unperturbed" state, with an ideal state having ΔT values near 0.

The effective Dunham parameters for the [15.30]1 state should be interpreted with caution. Because only two vibrational levels of this state were rotationally analyzed, effective parameters determined in the fit are more accurately T_0 than Y_{00} and $\Delta G_{1/2}$ than Y_{10}. This difference will inherently lead to small discrepancies between predicted and observed isotopologue shifts in T_v. The isotopologue dependence of the T_v values was decoupled from the Dunham model using ΔT parameters for all minor isotopologues for v=0,1.

In the final fit, the v=0-1 levels of the [15.30]1 state and the v=0-1 levels of the [14.26]0^+ state were fit using a Dunham model. The most abundant WS isotopologue, $^{184}W^{32}S$, was modeled using the Y_{00}, Y_{10}, Y_{20}, Y_{30}, … parameters. These Y_{lm} parameters were mass scaled for each isotopologue, and a ΔT was included to decouple the T_v values of the minor isotopologues from the Dunham parameters in the fit. Line positions for the ^{183}WS isotopologue were not measured in the spectrum of the (0,0) band of the [14.26]0^+– $X(0^+)$ transition due to its low intensity, and thus parameters for this isotopologue were not determined. For the v=2-3 levels of the [14.26]0^+ state, the ΔT parameter was included for the $^{184}W^{32}S$ reference isotopologue as well, decoupling the vibrational energies of these levels from the Dunham fit. This results in 13 ΔT parameters for the [14.26]0^+ state (^{182}WS, ^{183}WS, and ^{186}WS for v=0-3) and 6 ΔT parameters for the [15.30]1 state, as shown in Table 3.

Λ-doubling parameters for the [15.30]1 state, q_v and q_{Dv} were incorporated into the Dunham model. They were constrained to follow the mass relationship resulting from the pure precession approximation from Townes and Schalow[22] for a $^3\Pi_1$ state:

$$q_v = \frac{4B_v^2}{\Delta E} \quad (6)$$

where B_v is the rotational constant for a given vibrational level, and ΔE represents the separation between the two states involved in the "pure precession." Because the q_v parameter is proportional to B^2, we know the mass scaling of the parameter should follow as:

$$q_v^i = q_v^p\left(\frac{\mu_p}{\mu_i}\right)^2 \quad (7)$$

$$q_{D_v}^{i} = q_{D_v}^{p}\left(\frac{\mu_p}{\mu_i}\right)^3 \tag{8}$$

where the superscript *i* refers to a minor isotopologue, and the superscript *p* refers to the reference isotopologue, $^{184}W^{32}S$, and μ is the reduced mass.

In total, 5,201 observations were fit to 88 parameters with an average error of 0.004 cm^{-1}. The bandhead region of the experimental spectrum for the perturbed (1,0) band of the [15.30]1 – $X(0^+)$ transition, along with the PGOPHER[11] simulation, is shown in Figure 3. The determined Dunham fit parameters for the three electronic states, L-uncoupling values, and the ΔT and Λ-doubling parameters, are given in Tables 1-4, with Table 1 including a comparison of values for the current analysis to the previous set of Dunham parameters determined for the ground state.[7]

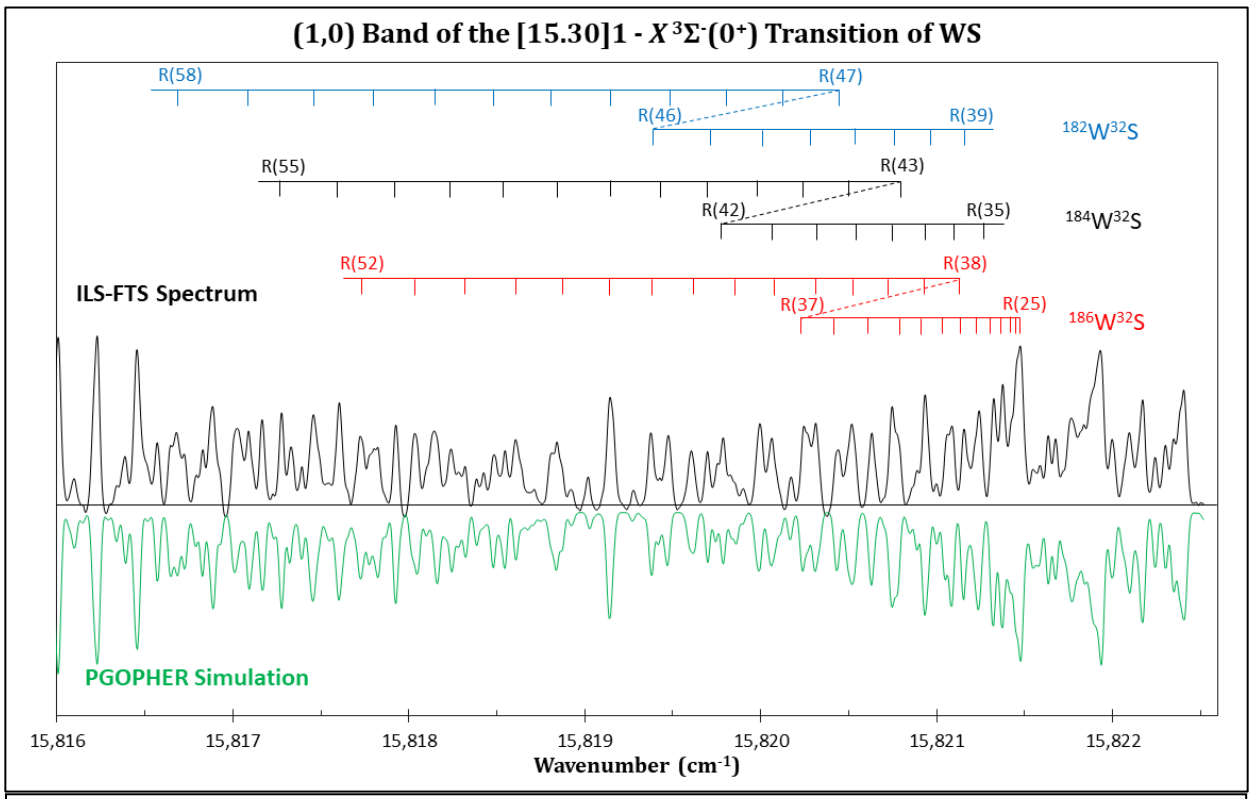

Figure 3. A portion of the experimental ILS-FTS spectrum for the (1,0) band of the [15.30]1 – $X(0^+)$ transition (black), with inverted PGOPHER[11] simulation (green) for comparison. A temperature of 600 K and a Gaussian linewidth of 0.025 cm^{-1} were used in the simulation. At the right side of the figure, four distinct bandheads are observable, due to the vibrational shift among the four major isotopologues: $^{186}W^{32}S$, $^{184}W^{32}S$, $^{183}W^{32}S$, and $^{182}W^{32}S$, with the bandhead corresponding to $^{182}W^{32}S$ appearing furthest to the right. Also shown are line positions for the perturbed R-branch of each of the three most abundant isotopologues in the region where energy levels for the two interacting [15.30]1 and [14.26]0^+ states cross and cause a sudden shift to higher energy within the branch.

Table 1. Dunham parameters for the $X\,^3\Sigma^-(0^+)$ state of WS. Parameters from this work are presented in regular typeface and parameters from our previous work are presented in *red italics*. Uncertainties are provided as (1σ). Here, the fitting uncertainty applies to $^{184}W^{32}S$, and the uncertainties for the other isotopologues are determined from those values. All values are in cm^{-1}.

$X\,^3\Sigma^-(0^+)$	$^{182}W^{32}S$	$^{183}W^{32}S$	$^{184}W^{32}S$	$^{186}W^{32}S$
Y_{00}	0[a]	0[a]	0[a]	0[a]
Y_{10}	561.05171 (75) *560.92910 (28)*	560.82203 (75) *560.69947 (28)*	560.59506 (75) *560.47255 (28)*	560.14773 (75) *560.02531 (28)*
Y_{20}	-1.97803 (76) *-1.87292 (14)*	-1.97641 (76) *-1.87139 (14)*	-1.97481 (76) *-1.86987 (14)*	-1.97166 (76) *-1.86689 (14)*
Y_{30}	0.02500 (21) -	0.02497 (21) -	0.02494 (21) -	0.02488 (21) -
Y_{01}	0.14528511 (69) *0.14529778 (79)*	0.14516618 (69) *0.14517884 (79)*	0.14504870 (69) *0.14506135 (79)*	0.14481731 (69) *0.14482994 (79)*
$Y_{11} \times 10^3$	-0.53287 (17) *-0.5572 (18)*	-0.53222 (17) *-0.5565 (18)*	-0.53157 (17) *-0.5558 (18)*	-0.53030 (17) *-0.5545 (18)*
$Y_{21} \times 10^3$	- *0.00826 (61)*	- *0.00825 (61)*	- *0.00824 (61)*	- *0.00821 (61)*
$Y_{02} \times 10^6$	-0.03809 (14) *-0.037964 (88)*	-0.03803 (14) *-0.037902 (87)*	-0.03797 (14) *-0.037841 (87)*	-0.03785 (14) *-0.037720 (87)*
$Y_{12} \times 10^9$	-0.100 (21) *-0.152 (16)*	-0.100 (21) *-0.152 (16)*	-0.100 (21) *-0.152 (16)*	-0.100 (21) *-0.151 (16)*
$Y_{03} \times 10^{12}$	-0.0447 (88) *-0.0263 (68)*	-0.0446 (88) *-0.0262 (67)*	-0.0445 (88) *-0.0261 (67)*	-0.0443 (88) *-0.0260 (67)*

[a]Held fixed in the fit.

Table 2. Dunham parameters for the [14.26]0+ and [15.30]1 states of WS. Uncertainties are provided as (1σ). All values are in cm^{-1}.

[14.26]0^+	**$^{182}W^{32}S$**	**$^{183}W^{32}S$**	**$^{184}W^{32}S$**	**$^{186}W^{32}S$**
Y_{00}	14,282.07147 (47)	14,282.07147 (47)	14,282.07147 (47)	14,282.07147 (47)
Y_{10}	524.134918 (60)	523.920351 (60)	523.708311 (60)	523.290411 (60)
Y_{20}	-1.17933 (26)	-1.17836 (26)	-1.17741 (26)	-1.17553 (26)
Y_{01}	0.13895109 (87)	0.13883735 (87)	0.13872499 (87)	0.13850368 (87)
$Y_{11} \times 10^3$	-0.41529 (60)	-0.41478 (60)	-0.41428 (60)	-0.41329 (60)
$Y_{21} \times 10^3$	-0.00497 (15)	-0.00496 (15)	-0.00495 (15)	-0.00493 (15)
$Y_{02} \times 10^6$	-0.03888 (17)	-0.03881 (17)	-0.03875 (17)	-0.03863 (17)
$Y_{12} \times 10^9$	0.344 (81)	0.344 (81)	0.343 (81)	0.342 (81)
[15.30]1	**$^{182}W^{32}S$**	**$^{183}W^{32}S$**	**$^{184}W^{32}S$**	**$^{186}W^{32}S$**
Y_{00}	15,320.20387 (49)	15,320.20387 (49)	15,320.20387 (49)	15,320.20387 (49)
Y_{10}	519.04300 (42)	518.83052 (42)	518.62054 (42)	518.20670 (42)
Y_{01}	0.14004139 (79)	0.13992676 (79)	0.13981352 (79)	0.13959048 (79)
$Y_{11} \times 10^3$	-0.35647 (32)	-0.35603 (32)	-0.35560 (32)	-0.35475 (32)
$Y_{02} \times 10^6$	-0.02957 (17)	-0.02952 (17)	-0.02947 (17)	-0.02938 (17)
$Y_{12} \times 10^9$	-1.558 (50)	-1.555 (50)	-1.552 (50)	-1.546 (50)
$Y_{03} \times 10^{12}$	-0.087 (10)	-0.087 (10)	-0.087 (10)	-0.087 (10)
$q_0 \times 10^3$	0.00102 (19)	0.00102 (19)	0.00102 (19)	0.00102 (19)
$q_1 \times 10^3$	0.01490 (34)	0.01488 (34)	0.01483 (34)	0.01490 (34)
$q_{D0} \times 10^9$	0.471 (27)	0.470 (27)	0.468 (27)	0.471 (27)
$q_{D1} \times 10^9$	0.724 (65)	0.722 (65)	0.719 (65)	0.724 (65)

Table 3. Magnitude of ΔT parameters for the [14.26]0^+ and [15.30]1 states of WS. Analysis of the v=0 vibrational level of the [14.26]0^+ state did not include the $^{183}W^{32}S$ isotopologue. Where a value is given for the $^{184}W^{32}S$ isotopologue, the vibrational energy is completely decoupled from the Dunham model. Where no value is given for $^{184}W^{32}S$, the central isotopologue does fit using the Dunham model, but the other isotopologues are decoupled from $^{184}W^{32}S$. All values are in cm^{-1}.

[14.26]0^+	**$^{182}W^{32}S$**	**$^{183}W^{32}S$**	**$^{184}W^{32}S$**	**$^{186}W^{32}S$**
v=0	0.03980 (49)	-	-	-0.03397 (47)
v=1	0.03579 (31)	0.01693 (39)	-	-0.03034 (33)
v=2	0.5640 (14)	0.5473 (14)	0.5318 (13)	0.5046 (13)
v=3	1.5383 (33)	1.5031 (33)	1.4817 (34)	1.4545 (32)
[15.30]1	**$^{182}W^{32}S$**	**$^{183}W^{32}S$**	**$^{184}W^{32}S$**	**$^{186}W^{32}S$**
v=0	0.03062 (32)	0.01440 (36)	-	-0.03240 (32)
v=1	0.04619 (37)	0.02401 (43)	-	-0.04326 (37)

Table 4. L-uncouple operator values for the interactions between [15.30]1 v=0 and [14.26]0^+ v=2 and for [15.30]1 v=1 and [14.26]0^+ v=3. These operator values were constrained to a single value for all four isotopologues.

Interacting States	L-uncouple Value
[15.30]1 v=0 **[14.26]0^+ v=2**	0.0063893 (93)
[15.30]1 v=1 **[14.26]0^+ v=3**	0.010301 (13)

4. DISCUSSION

The deperturbation analysis of the (1,0) and (0,0) bands of the [15.30]1-$X(0^+)$ transition was able to model the isotopologue dependent rovibrational structure quite effectively. Experimental observations of the perturbed rotational branches are reproduced by the simulation to experimental accuracy. The Dunham-like model used in the final fit of the observed transitions serves as a second check for the effectiveness of the deperturbation analysis. If the perturbation is modeled effectively, the "ideal" potential energy curves for the interacting states can be approximated. The Dunham model applies to smooth potential energy surfaces, such as those for isolated electronic states. While the electronic structure of WS is quite dense and Hund's Case (c) is certainly applicable, if the primary interaction results from only two states then a successful deperturbation should result in potential energy curve that could be well modeled by a Dunham expansion.

A Dunham-like model was used describe the three electronic states involved in the observed transitions: $X0^+$, [14.26]0^+, and [15.30]1. The obtained parameters (see equations 1-5) are presented in Table 1 for the $X(0^+)$ state and Table 2 for the excited states. These tables can be used to evaluate the legitimacy of the obtained Dunham potentials. For a given series of Y_{lm} values, we see a sharp decrease in magnitude as l increases, which is expected for a Taylor series expansion. For example, there are 3 orders of magnitude differences between Y_{01} and Y_{11}, with a further 2 orders of magnitude differences between Y_{11} and Y_{21} for the [14.26]0^+ state. This suggests that the expansion of B_v is converging to zero and that the Dunham parameters are modeling the vibrational dependence of the rotational constant effectively. We can also evaluate whether known relationships between other parameters are preserved. The Kratzer relationship[16] gives the expected relationship between Y_{02}, Y_{01}, and Y_{10}:

$$Y_{02} = -\frac{4Y_{01}^3}{Y_{10}^2} \quad \rightarrow \quad D_e = \frac{4B_e^3}{\omega_e^2} \tag{9}$$

Calculating an expected Y_{02} from experimentally determined values of Y_{01} and Y_{10} for $^{184}W^{32}S$ of the [14.26]0^+ state, we find a value of -3.89 x 10^{-8} cm^{-1}, which compares to the fit Y_{02} parameter of -3.87 x 10^{-8} cm^{-1}. A similar comparison for the [15.30]1 state finds a calculated Y_{02} value of -4.06 x 10^{-8} cm^{-1} and a fit value of -2.97 x 10^{-8} cm^{-1}. While there is a larger discrepancy between these two latter values, the difference is reasonable due to the slightly larger uncertainty

in the Y_{10} value, which is actually $\Delta G_{1/2}$ rather than ω_e (see above). A similar comparison may be made using the Pekeris relationship[16]

$$Y_{20} = -Y_{01}\left(\frac{-Y_{11}Y_{10}}{6Y_{01}^2}+1\right)^2 \quad \rightarrow \quad \omega_e\chi_e = B_e\left(\frac{\alpha_e\omega_e}{6B_e^2}+1\right)^2 \tag{10}$$

where the calculated value for Y_{20} of -1.15 cm^{-1} compares quite favorably to the fitted value of -1.18 cm^{-1}. These relationships indicate that the deperturbation analysis was quite effective in producing "ideal" unperturbed potential energy wells of the two interacting states.

The initial experimental analysis of the $[14.26]0^+$ state by our group described the v=0 and v=1 vibrational levels[7] and was extremely valuable in providing accurate predictions for parameters of the v=2 vibrational level. This deperturbation analysis would have been difficult if not impossible without these initial values which were used early in the analysis to model perturbation effects and assist with line assignments in the heavily perturbed regions. Extrapolating from the v=0 and v=1 levels provided a T_2 value roughly 1 cm^{-1} from the experimentally determined value, and a provisional B_2 value that was within 2 x 10^{-5} cm^{-1} of the determined value. This is reflected in the relative magnitude of the ΔT values from the fit presented in Table 3. The consistency observed here provides further validation that the assignment of the perturbing states are correct.

The earlier analysis of the [15.30]1 transition by Zhang, *et al.*[4] was limited by the low experimental temperature used in LIF measurements which allowed inclusion of only low-J lines. This limitation prevented observation of the perturbation at higher J and only one isotopologue, $^{184}W^{32}S$, was able to be characterized. However, our results do show good agreement to the previous findings, with our T_0 and B_0 values falling within their experimental error. The main difference between the two studies' findings is in the determination for D_0, in which the previously determined value[4] is negative. Our positive D_0 value is more plausible, as D is the centrifugal distortion constant and is used to account for the increase in bond length and moment of inertia experienced by the molecule as rotational velocity increases. A negative D value would suggest a decreasing bond length with increasing rotational energy.

Additional comparisons can be made to the *ab initio* results given by Tsang *et al.*[3] Predicted equilibrium constants are compared to the corresponding experimentally determined values for the central $^{184}W^{32}S$ isotopologue from the current work in Table 5. Here, the label given to the *ab initio* electronic states is determined by rank of a given Ω-value, i.e., $\{5\}0^+$ is fifth highest $\Omega=0^+$ state predicted. Correlation between experimental and *ab initio* states is based heavily upon B_e and ω_e values due to the difficulty in prediction of term energy (T_e) among a dense population of states. While the relative ordering of the levels tends to be well-predicted, a somewhat regular correction to the energy value must often be applied. Previous works[3,5,7] have correlated the $[14.26]0^+$ state to the *ab initio* $\{5\}0^+$ state, however, we find that aside from a larger discrepancy in T_e, the $\{6\}0^+$ state is a better fit for all other determined constants. In addition, this work has the added benefit of giving more insight into the Λ-S character of the involved states due to the selection rules associated with perturbation effects. As previously mentioned, an L-uncouple interaction requires that the two perturbing states have $\Delta S=0$, $\Delta\Omega=\pm1$

and $\Delta\Lambda=\pm1$. The [15.30]1 state, correlated to the *ab initio* {10}1, is expected to be predominantly $^3\Sigma^-$ (55%) in character, while $\{5\}0^+$ and $\{6\}0^+$ are predicted to be $^5\Delta$ (76%) and $^3\Pi$ (85%), respectively.[3] Re-assigning the $[14.26]0^+$ state to $\{6\}0^+$ would satisfy the selection rules for the perturbation which allow interaction to occur.

Table 5. Equilibrium constants for $^{184}W^{32}S$ determined by this work (regular typeface) and by computational prediction[3] *(red italics)*. While previous works correlated the $[14.26]0^+$ state to $\{5\}0^+$, we suggest a re-assignment to $\{6\}0^+$.

$^{184}W^{32}S$	T_e (cm^{-1})	B_e (cm^{-1})	r_e (Å)	ω_e (cm^{-1})	$\omega_e\chi_e$ (cm^{-1})
$[14.26]0^+$	14,282	0.1387	2.112	523	1.2
{5}0⁺	*14,464* [a]	*0.1339* [a]	*2.152* [a]	*506* [a]	*7.7* [a]
{6}0⁺	*15,269* [a]	*0.1375* [a]	*2.122* [a]	*526* [a]	*2.3* [a]
[15.30]1	15,320	0.1398	2.104	519	-
{10}1	*17,108* [a]	*0.1380* [a]	*2.116* [a]	*559* [a]	*5.7* [a]

[a] Ref [3]

5. CONCLUSION

Although both states have been described previously in the literature, the availability of high-resolution spectra at sufficient temperature for observation of high J lines has allowed this analysis to provide a significant addition to our understanding of the $[14.26]0^+$ and [15.30]1 states of WS. Lines from all four abundant isotopologues of WS were observed in the (0,0) and (1,0) bands of the [15.30]1 – $X(0^+)$ transition, which were rotationally analyzed using PGOPHER.[11] Because these bands were significantly perturbed by a nearby electronic state, this analysis also provides insight into the interaction of two states in an electronically complex molecule. The two bands were shown to be perturbed by the v=2 and v=3 vibrational levels of the $[14.26]0^+$ state, of which the v=0 and v=1 levels were analyzed by our group in a prior work.[7] Parameters predicted from the previous work, as well as lines observed for the (2,0), (2,1), and (3,0) bands of the $[14.26]0^+$ - $X(0^+)$ transition aided in completion of a deperturbation analysis. This resulted in the determination of an L-uncouple parameter for each interaction. The deperturbation analysis used the constrained-variables approach from Breier *et al.*[14] to fit the [15.30]1, $[14.26]0^+$, and $X(0^+)$ states to a mass-independent Dunham[13] model in PGOPHER.[11] An additional parameter, labeled ΔT, was included as needed to decouple the vibrational energies of the minor isotopologues of the [15.30]1 state and all isotopologues of the $[14.26]0^+$ state from the Dunham model. Finally, examination of equilibrium constants as well as the predicted Λ-S character of the two perturbed states resulted in a re-assignment of the $[14.26]0^+$ state to the *ab initio* $\{6\}0^+$ state.

Supplementary Materials

The following files are provided for the reader: an input file (WS Inp_File.lin), containing the constraints, experimental line positions, and fit instructions; a PGOPGHER**Error! Bookmark**

not defined. file (WS 15t30 Deperturbation with Dunham Final.pgo); and spectral data file (WS [15.30] Overlays.ovr) containing the concatenated ILS spectra, processed FTS spectrum, and the output file (Dunham 14.26 and 15.30 – Final.txt).

Acknowledgements

This work was supported by the National Science Foundation, Grant Nos. CHE-1955773 (JOB) and CHE-1955776 (LOB).

REFERENCES

1. B. Liang, L. Andrews, J. Phys. Chem. A **106** (2002) 6945-6951.
2. A. Sevy, R.F. Huffaker, M.D. Morse, J. Phys. Chem. A **121** (2017) 9446–9457.
3. L.F. Tsang, M.-C. Chan, W. Zou, A.S.-C. Cheung, J. Mol. Spectrosc. **359** (2019) 31–36.
4. J. Zhang, F. Fang, L. Zhang, D. Zhao, X. Ma, J. Yang, J. Mol. Spectrosc. **366** (2019) 111223.
5. J. Zhang, W. Zou, L. Zhang, D. Zhao, X. Ma, J. Yang, J. Quant. Spectrosc. Radiat. Transfer **256** (2020) 107314.
6. J.C. Harms, B.M. Ratay, K.N. Bales, J.J. O'Brien, L.C. O'Brien, J. Mol. Spectrosc. **372** (2020) 111349.
7. J.C. Harms, K.N. Bales, J.J. O'Brien, L.C. O'Brien, J. Mol. Spectrosc. **374** (2020) 111378.
8. K.N. Bales, J.C. Harms, J.J. O'Brien, L.C. O'Brien, J. Mol. Spectrosc. **377** (2021) 111430.
9. B. Groven, M. Heyne, A.N. Mehta, H. Bender, T. Nuytten, J. Meersschaut, T. Conard, P. Verdonck, S. Van Elshocht, W. Vandervorst, S. De Gendt, M. Heyns, I. Radu, M. Caymax, and A. Delabie, Chem. Mater. **29** (2017) 2927-2938.
10. M.K.S. Bin Rafiq, N. Amin, H.F. Alharbi, M. Luqman, A. Ayob, Y. S. Alharthi, N.H. Alharthi, B. Bais, and M. Akhtaruzzaman, Sci. Rep. **10** (2020) 771.
11. PGOPHER, A Program for Simulating Rotational, Vibrational and Electronic Spectra, C. M. Western, JQSRT **186** (2017) 221–242. doi:10.1016/j.jqsrt.2016.04.010. (version 11.0.141.0).
12. H. Lefebvre-Brion, R.W. Field, Perturbations in the Spectra of Diatomic Molecules, Elsevier, 1986.
13. J.L. Dunham, Phys. Rev. **41** (1932) 721.
14. A.A. Breier, B. Waßmuth, T. Büchling, G.W. Fuchs, J. Gauss, T.F. Giesen, J. Mol. Spectrosc. **350** (2018) 43.
15. L.C. O'Brien, J.C. Harms, J.J. O'Brien, W. Zou, J. Mol. Structure **1211** (2020) 128024.
16. P.F. Bernath, Spectra of Atoms and Molecules, third ed., Oxford University Press, New York, NY, 2016.
17. H. Salami, A.J. Ross, A molecular iodine atlas in ascii format, J. Mol. Spectrosc. **223** (2005) 157–159.
18. J.C. Harms, J.J. O'Brien, L.C. O'Brien, J. Chem. Phys. **148** (2018) 204306.
19. F. Kerber, G. Nave, and C.J. Sansonetti. Astrophys. J., Suppl. Ser. **178** (2008) 374-381.
20. I.E. Gordon, L.S. Rothman, C. Hill, et al., The HITRAN2016 molecular spectroscopic database, JQSRT **203** (2017) 3–69.
21. J.M. Brown, E.A. Colburn, J.K.G. Watson, F.D. Wayne. J. Mol. Spectrosc. **74** (1979) 294-318.
22. C.H. Townes, A.L. Schawlow, Microwave Spectroscopy, 1st Ed, Dover Publications, Inc., pp 188-192, 1975.